Verifiable Smart Packaging with Passive RFID

Ge Wang[†], Chen Qian[*], Jinsong Han[†‡],Wei Xi[†], Han Ding[†],Zhiping Jiang[†],Jizhong Zhao[†]
[†]Xi'an Jiaotong University, China
[*] University of California Santa Cruz, USA
[‡]Carnegie Mellon University, USA

Abstract

Smart packaging adds sensing abilities to traditional packages. This paper investigates the possibility of using RF signals to test the internal status of packages and detect abnormal internal changes. Towards this goal, we design and implement a nondestructive package testing and verification system using commodity passive RFID systems, called Echoscope. Echoscope extracts unique features from the backscatter signals penetrating the internal space of a package and compares them with the previously collected features during the check-in phase. The use of backscatter signals guarantees that there is no difference in RF sources and the features reflecting the internal status will not be affected. Compared to other nondestructive testing methods such as X-ray and ultrasound, Echoscope is much cheaper and provides ubiquitous usage. Our experiments in practical environments show that Echoscope can achieve very high accuracy and is very sensitive to various types abnormal changes.

Categories and Subject Descriptors

C.2.m [[**Computer System Organization**]]: Computer Communications Networks

Keywords

Smart packaging; Wireless sensing; RFID

1. INTRODUCTION

Identifying and tracking items is a crucial task for various automatic management systems with applications of logistics, supply chain, and retailing. Towards this purpose, Radio Frequency Identification (RFID) systems have been developed and widely utilized. An RFID tag attached to the surface of an item serves as the label to identify the item and can be recognized by an RFID reader. RFID-based smart packaging systems has been proposed. However, the essential mechanism of RFID-based smart packaging is to identify the tags rather than the items inside packages. Consider these cases in an RFID-based logistic system. An intruder may steal the items in a tagged package or replace the expensive items by cheap ones. A terrorist may add bombs to an ordinary baggage during transportation. RFID systems have no ability to detect such malicious behaviors that change the internal status of tagged packages[1]. Hence testing and verifying the internal status of packages is of importance for the authenticity, integrity, and safety of automatic management systems. In this paper, we target on the problem of verifying the internal status of packages and detecting abnormal changes of the internal items.

Obviously physical inspection that requires opening the packages is slow and labor-intensive. Instead, nondestructive testing that evaluates the packages without causing any physical changes to them is more preferred. However, prior solutions for nondestructive testing is not suitable for testing the internal status and changes of containers, as listed below.

- X-ray screening: X-ray screening is a image-based method that can graphically reveal the internal details of a package. However, X-ray devices are usually expensive. In addition, image-based methods may compromise the privacy of customers and image-based features are easier to simulate. Attackers may cheat the system by replacing with same-shaped items according to the feature of X-ray images.
- Ultrasonic testing: Ultrasonic testing requires special and costly equipment. The requirement on extra hardware and manual process limits the deployment in real practice.
- Seal tag: a simple solution is to put a seal tag onto the package, which can not be opened without breaking the seal tag. However, this approach still only verifies the seal tag rather than the internal objects. In practice, it is possible that an attacker uses physical approaches to cheat the testing system. For example, an attacker may open the package and use a forged seal tag with the same ID or barcode to re-pack the package.
- Weighing: another simple idea is to weigh the package at all testing locations to find any difference in weight. Though being cost-efficient, this method can be easily cheated by replacing original items with cheap weighting material.

[1]Hereafter we use "package" to refer to any types of containers.

UbiComp '16, September 12-16, 2016, Heidelberg, Germany
© 2016 ACM. ISBN 978-1-4503-4461-6/16/09…$15.00
DOI: http://dx.doi.org/10.1145/2971648.2971692

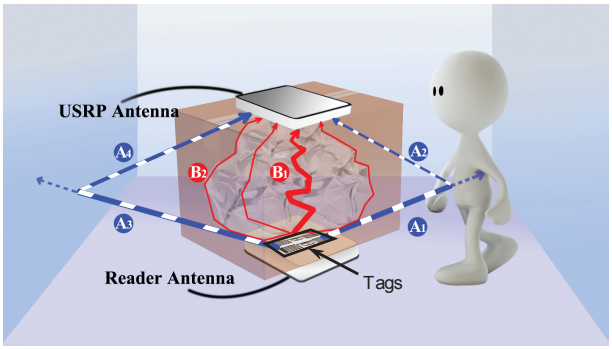

Figure 1: Overview of Echoscope

To our knowledge, no existing work has successfully used RF signals for internal status checking and verification of a package. In this work we investigate the possibility of RF-based low-cost and nondestructive testing. The key idea of RF-based nondestructive testing is to extract distinct features from the signal penetrating the internal space of a package. However, using RF signals to identify the internal structure like X-rays is difficult. Different from X-rays, RF wavelengths are too long to delicately depict the shapes of the items inside the package, and the different absorption rates for different materials using RF signals can hardly be recognized. RF-based testing cannot produce images like those in X-ray screening.

In our application scenarios, an automatic management system always has a check-in site where the identifier (such as barcode or the tag ID) and other features of a packages can be collected and stored in a database. Then at another testing site, different from the check-in site, the testing system should be able to verify whether the internal status inside the package have been changed. *We assume packages are tightly filled and packed.* Hence items can hardly be relocated inside a package.

Since at a testing site we only require to *verify* whether the internal status of a packages is changed, the testing system does not need to identify the shapes and material of the items in a package. It only needs to determine whether the ID and signal features collected at a testing site match the original record. However, directly using the power of RF signals sent from a normal transmitter (such as WiFi) for nondestructive testing is still impractical, because the differences among radio sources and environments at different sites may cause different RF signal features and result in false acceptance or false rejection in testing results.

To resolve these challenges, we propose to utilize *backscatter communication* of passive RFID systems as the RF source for nondestructive testing. The proposed system Echoscope is built using commodity off-the-shelf (COTS) RFID readers and tags. The structure of Echoscope is shown in Fig. 1. For each package, we paste *a pair of tags* in parallel at the center of its inner-bottom side. At the check-in and testing sites, the package is placed on top of an RFID reader. In addition we deploy a monitor with a Universal Software Radio Peripheral (USRP) model N210 at the top of the package to collect the RF signals from the reader and tags.

At the check-in site, for each package Echoscope collects the RF signals of backscatter communication between the tags and reader and stores them in a database. At a different testing site, Echoscope repeats the signal collection step and compares the extracted features with the record in the database.

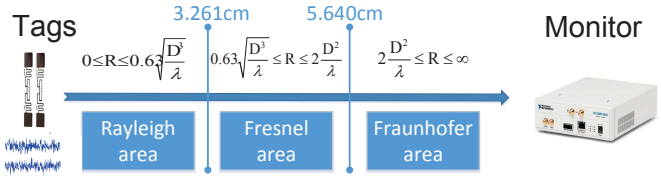

Figure 2: Backscatter signal areas

We have implemented prototype systems of Echoscope and conducted extensive experiments. The evaluation results in various environments show that Echoscope exhibits a high accuracy in detecting abnormal changes for a large variety of items. The false accept rate of Echoscope using three types of RFID tags is as low as 4.76% in average.

The remaining paper is organized as follows. We present the system model in Section 3 and the detailed design in Section 4. In Section 5 we describe the implementation of Echoscope and show the experiment results. We introduce the related work in Section 7. In the end we conclude this work in Section 9.

2. BACKGROUND

An RFID system using passive tags relies on backscatter communication. A reader interrogates passive tags by broadcasting RF signals. A tag, which is battery-free, backscatters the RF wave impinging to its antenna. The EPC C1G2 protocol [6] is a mainstream air protocol based on slotted ALOHA, widely used for backscatter communication in RFID systems. Echoscope is compatible to this protocol and only uses the "ID" segments of tag replies.

Suppose an RF signal penetrates the internal space of a package and is received by the monitor above the package. According to the electromagnetic wave propagation principle introduced in [8], the space of a signal propagation can be divided into three areas, namely the Rayleigh, Fresnel, and Fraunhofer areas. The propagation characteristic of the RF signal is totally different in the three areas. The passive RFID tags used in this work have a maximum aerial diameter of 9.5cm and the wave length of the RF waves is 32cm. The boundary between the Fresnel area and Fraunhofer areas is about 5.640cm away from the tag (as shown in Fig. 2). Assuming all packages are taller than 5.64cm, the backscattered RF signals of this tag received by the USRP monitor are all in the Fraunhofer area. In this area, the power P of the backscattered RF signals at a certain position is mainly influenced by the permittivity ε according to Poynting's theorem [8]. Also ε is essentially determined by the material and shape of the items inside a package. Based on this insight Echoscope can decide whether the internal status of a package has been changed based on the analysis of the RF signals penetrating the package.

3. BASIC IDEA AND EXPERIMENTAL VALIDATION

In this section, we present the basic idea of Echoscope to extract features from backscatter signals.

3.1 Feature source selection

A sequence of radio signal received by the monitor of Echoscope includes three components: basic signal from the radio source, noise caused by environmental factors, and signal changes caused by the propagation medium in the packet internal space. The essential goal of Echoscope is to extract the feature of RF signals penetrating the internal space while eliminating the environmental noise. We choose to extract features from tag backscatter signals. This approaches matches well to the requirements of Echocope due to the following considerations. First, the tags attached to the package are consistent signal sources at different sites. Hence signal changes introduced by differences among devices are minimized in the feature extraction process. We only need to eliminate environmental noise. Second, all tag responses follow the same order, *e.g.*, the *ID* of every tag consists of *PC*, *EPC*, and *CRC* in the sequential order. This property ensures that whenever and wherever we test the package, the tags can provide consistent signals from the sources. Although these signals may still be different due to the difference among the packet internal space and the environment of the testing sites, we may use advanced strategies to extract the features that are caused by the packet internal status only. We will introduce how we eliminate environmental noise in the next subsection.

3.2 Reduction of Environmental Noise

When the signal sources are identical, the next step is to eliminate or reduce the environmental noise. Our important design choice is to use *a pair of tags* instead of a single one to eliminate the noise and extract the packet internal feature. In this section, we first propose a theoretical model showing how we use a pair of tags to reduce noise and then we demonstrate our experimental results that validate the proposed model.

As shown in Fig.1, the signal backscattered from a tag mainly experiences three propagation effects, *i.e.*, reflection, diffraction, and refraction, before it reaches the monitor antenna. We decompose a backscatter signal received by the monitor into two categories, namely the *characteristic* and *noisy* parts. As shown in Figure 1, the characteristic part, marked in red color(line $B1 \sim B2$), convey the features of the internal status of the package. They mainly comprise of the refracted and diffracted signal by the inside items and package. The noisy part, marked in blue color(line $A1 \sim A4$), do not provide any feature information about the package. They are mainly reflected by the environment. Hence Echoscope needs to extract features from the characteristic signal. However, it is challenging to eliminate noisy signal by reading only a single tag.

We propose to solve this problem by placing two tags at the inner-bottom side of each package. We use F and N_{en} to represent the characteristic and noisy parts of the signal respectively. Given two tags, tag 1 and tag 2, in a package, the received signals at the monitor, denoted as S_1 and S_2, can be represented as follows.

$$\begin{aligned} S_1 &= ID_1 + T_1 + F_1 + N_{en} + N_{eq} + N_w \\ S_2 &= ID_2 + T_2 + F_2 + N'_{en} + N'_{eq} + N'_w \end{aligned} \tag{1}$$

Here ID_1 and ID_2 are the ID information of both tags, in the sequence $(PC + EPC + CRC)$. T_1 and T_2 are the signal part caused by hardware characteristics of the two tags. N_{eq} and N'_{eq} are the noise introduced by the monitor, and N_w and N'_w are white Gaussian noise.

If we compute the difference between S_1 and S_2, we have:

$$\begin{aligned} S_1 - S_2 =& (ID_1 - ID_2) + (T_1 - T_2) + (F_1 - F_2) \\ &+ (N_{en} - N'_{en}) + (N_{eq} - N'_{eq}) + (N_w - N'_w) \end{aligned} \tag{2}$$

For a given pair of tags, $(ID_1 - ID_2)$ and $(T_1 - T_2)$ are always identical whenever the reader interrogates them. Moreover, the noises introduced by the monitor, denoted as N_{eq} and N'_{eq} for tag 1 and 2, are also similar at a same time. Then we may have:

$$S_1 - S_2 = C + (F_1 - F_2) + (N_{en} - N'_{en}) + (N_w - N'_w) \tag{3}$$

where $C = (ID_1 - ID_2) + (T_1 - T_2)$. Note that two noise signal vectors N_w and N'_w are independent to each other. Similarly, F_1 and N_w are independent, and F_2 and N'_w are also independent. Let $G = N_w - N'_w$. We have $G \sim N(0, \delta_{i'}^2 + \delta_{j_0}^2)$. If Echoscope collects sufficiently many signal samples from both of the two tags, according to the law of large numbers [7], the difference of the sum of $(N_w - N'_w)$ and the expectation of variable G is infinitely close to 0:

$$\lim_{n \to \infty} \sum [(N_w - N'_w)]/n - E(G) \leq \epsilon \tag{4}$$

Since $E[G] = 0$, we further have the following equation:

$$E[S_1 - S_2] = C + E[(F_1 - F_2) + (N_{en} - N'_{en})] \tag{5}$$

Since N_{en} and N'_{en} are introduced by two tags at very close positions, we conjecture that N_{en} is very similar to N'_{en}. It is based on an intuition that the distance between the two tags is much shorter than the distance from them to the objects in the environment. In other words, tags at very close positions may share very similar ambient noises and multipath effects. Prior researches, such as [20] and [12], have demonstrated this fact.

In fact if we can verify that $F_1 - F_2 \gg N_{en} - N'_{en}$, we can assume that the feature difference $(F_1 - F_2)$ plays a dominate role in the above equation. As a result, $\sum(S_1 - S_2)$ can then be considered as a valid feature source of the internal status of the package. We propose the following conjecture.

Conjecture. *Given a certain package tested by Echoscope in a random environment and the two tags are close to each other within a few centimeters. For feature signals F and F' and environmental noise N_{en} and N'_{en}, we have $F_1 - F_2 \gg N_{en} - N'_{en}$.*

We use experiments in real environments to verify the above conjecture. In addition, we also obtain this result from detailed theoretical modelling and analysis. Due to the page limit, we only present the experimental results.

We conduct two sets of experiments to estimate $N_{en} - N'_{en}$ and $F_1 - F_2$ respectively. In the first set of experiments, we intend to estimate $N_{en} - N'_{en}$ by eliminating the influence of tag hardware differences C as well as that of feature difference $F_1 - F_2$. The idea of the experiments is to use a same tag to make $C = 0$ and use a completely empty package to make $F_1 = F_2$. As shown in Fig.3(a), we first attach the tag to the inner-bottom side of the package with 2cm distance to the center and let the monitor collect 800 signal samples. Then we rotate the package for 180 degrees and make the tag on the other side, still with 2cm distance to the center. The monitor collects another 800 signal samples. The two sets of signal samples can be used to simulate a pair of identical tags with 4cm distance to each other. Since the package is

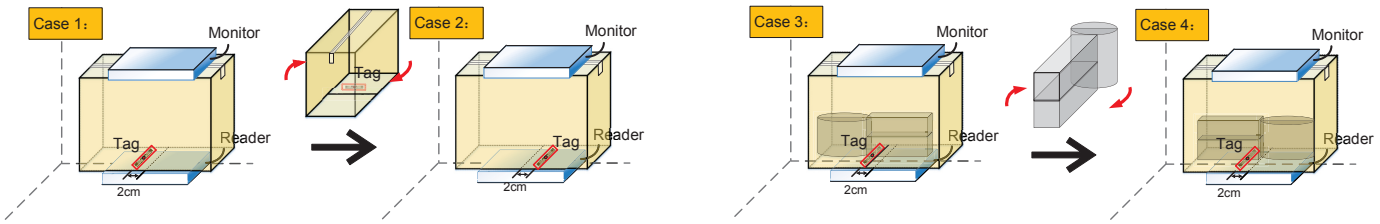

(a) Experiment 1 (b) Experiment 2

Figure 3: Two sets of experiments to validate $F - F' \gg N_{en} - N'_{en}$

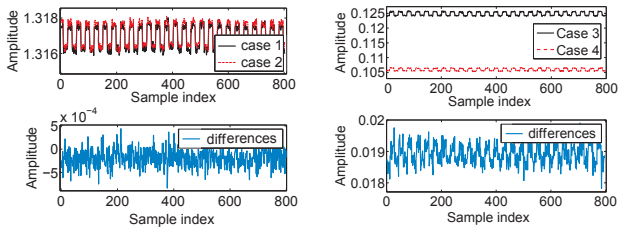

(a) Estimation of $N_{en} - N'_{en}$ (b) Estimation of $F - F'$

Figure 4: Estimation of $N_{en} - N'_{en}$ and $F - F'$

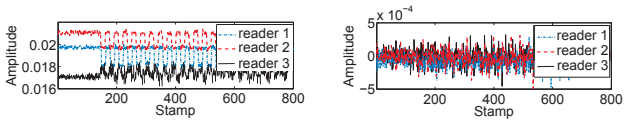

(a) Tag's signals for different readers (b) Differences between two adjacent signals

Figure 5: Subtraction eliminates reader features.

completely empty, we can assume that $\sum(F_1 - F_2) = 0$. Also $C = (ID_1 - ID_2) + (T_1 - T_2) = 0$ for a same tag. Therefore,

$$E[S_1 - S_2] = E[N_{en} - N'_{en}] \quad (6)$$

We show the two sets signal samples in the top figure of Fig. 4(a), as "case 1" and "case 2". Their difference is shown in the bottom one of Fig. 4(a). We find that the average amplitude of $S_1 - S_2$ is in the order of 10^{-4}, much smaller compared to the amplitude of S_1 and S_2 in the order of 1.

To estimate $(F_1 - F_2)$, we conduct another set of experiments. As shown in Fig. 3(b), we fill the package with some objects and let the monitor collect 800 signal samples. Then we relocate the objects in the package and make them as the mirror images to the original locations. Then the monitor collects another 800 signal samples. In the two experiments, the environment is maintained to be identical. Since the tag does not move in the two experiments, we may consider the environmental noise is very close, *i.e.*, $N_{en} - N'_{en} = 0$. Also $C = 0$. Hence,

$$E[S_1 - S_2] = E[F_1 - F_2] \quad (7)$$

In Fig. 4(b), the top figure shows the signal samples of S_1 and S_2 of the two sets of experiments. We can see that they differ significantly. The bottom figure shows their difference, *i.e.*, $S_1 - S_2$. The average difference, $E[S_1 - S_2] = E[F_1 - F_2]$, is in the order of 10^{-2}. Hence $E[F_1 - F_2]$ is larger than $E[N_{en} - N'_{en}]$ by about two orders of magnitude. We also try different materials to fill the package, including alloy, water, wood, clothes, and carton, and confirm that 10^{-2} is a normal value for $E[F_1 - F_2]$.

Our experiments validate the conjecture that $F_1 - F_2 \gg N_{en} - N'_{en}$, which means the dynamic component of $S_1 - S_2$ is dominated by the features of the package internal status, including the structure, material, and positions of the objects inside the package. In addition, we conduct similar experiments to estimate that the value of C is smaller than 10^{-3}. Due to the space limit, we skip the details.

Backscatter signals of passive tags reflect the hardware characteristics of both the reader and tags. We conduct a set of experiments to validate that the proposed substraction method is not affected by the variety of readers. We use three types of readers, *i.e.*, Impinj R220 (reader 1), Impinj R420 (reader 2) and Alien ALR9680 (reader 3), to interrogate an Impinj E41C tag at different sites.

We plot the results in Fig. 5. Fig. 5(a) presents the backscattering signals of the tag interrogated by different readers. We find that these signals are distinct. However, if we take the above subtraction and show the differences of signals from two adjacent signal segments of a same tag in Fig. 5(b). Here $F_1 - F_2 = 0$ because they are from a same tag. The differences are extremely small (in the order of 10^{-4}), which means the substraction method can eliminate features introduced by the reader and environments.

4. SYSTEM DESIGN

As shown in Fig. 6, Echoscope comprises of four modules, namely *Signal Collection*, *Noise Elimination*, *Feature Extraction*, and *Feature Matching*. In the Signal Collection phase, Echoscope records the raw signals of the backscatter communication from the tags to the reader using the USRP monitor. In the Noise Elimination phase, certain necessary processes are conducted to remove the noise from the raw signals. The Feature Extraction phase extracts features from the backscatter signals. The last module, Feature Matching, decides whether the features from the collected signals match the ones stored in the database.

4.1 Backscatter signal collection and segmentation

We use a *record* to denote the raw signal data recorded by the monitor within a time duration, including all signals sent from the reader and backscattered from the tags. During this time, the reader keeps querying the two tags and the monitor records the communication signals. The default duration of each record is 1 seconds. Hence a record includes multiple

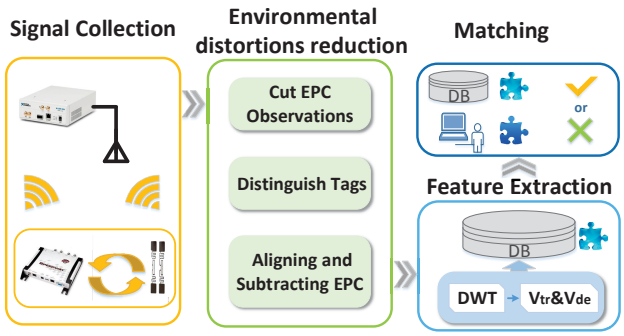

Figure 6: System workflow

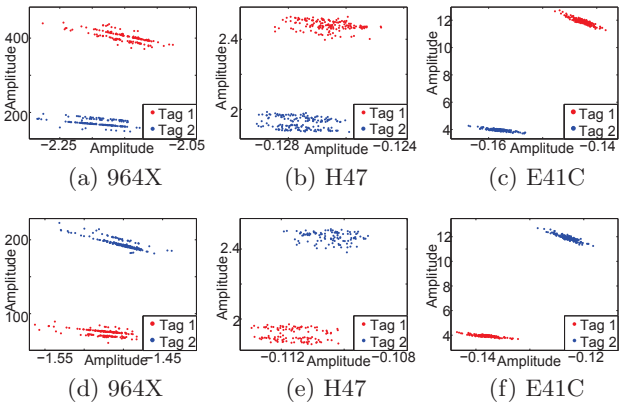

Figure 7: K-means clustering for observations of two tags after FFT: *(a)(b)(c) show the results of two tags with similar EPCs. (d)(e)(f) show those of two tags with significantly different EPCs*

rounds of backscatter communication. Let an *observation* to denote a part of backscatter signals in a record, *i.e.*, the part corresponding to the time duration between the end of an *ACK* and the start of an *QueryRep*. An observation contains the data of the *ID*, *i.e.*, *PC+EPC+CRC*. Echoscope only uses backscatter signals for testing, thus it should filter other RF signal parts.

To achieve this goal, Echoscope needs to identify the observations of a record to obtain the backscatter parts containing the *ID*s by performing accurate *segmentation* on the signal. It is difficult for current commodity readers to perform such operation because the API to analyze signals in detail is not open to public. Instead we utilize USRP N210 as the monitor [24] to record the communication process between the reader and tags. The monitor operates as a passive listener and records the electromagnetic signals.

If the *ID* field of a tag can be directly decoded from the signal captured by the monitor, it would be very easy to segment the signal to get an observation. However, when penetrating the internal space of a package the signals backscattered from tags are distorted and became very difficult to be decoded. Thus, we cannot obtain desired observations directly by decoding. Even if observations are successfully segmented, without ID information Echoscope still cannot identify which tag an observation belongs to. When each record is for 1s time duration, there could be over 100 observations. Hence how to quickly and accurately segment and identify that many observations is another challenge.

We thereby employ an indirect method for extracting observations. This method leverages the reader's signal, which has much higher signal strength than that of a tag. According to the EPC C1G2 specification, a tag replies its *ID* after it receives an *ACK* commend from the reader. Then the reader sends another command *QueryRep*. *ACK* and *QueryRep* have preambles of '01' and '00', respectively. By inspecting the signal amplitude from a record and recognizing the preambles of above reader commands, we can find out the edges of desired observations.

We utilize Backscatter link frequency (BLF), which is the frequency of a tag-to-reader link [6], to identify tags based on observations. Due to manufacturing imperfection, BLF determines a tag's responding data rate. It varies among different tags [13] and can be used as a "fingerprint". To extract BLFs from distorted signals, we perform Fast Fourier Transform (FFT) on the observations. We calculate the variance and mean values of the result after FFT, and map them to a two-dimensional plane. Those values can be further clustered in the plane by applying the K-means algorithm. In Fig. 7, we show the results of mapping and clustering about 360 observations monitored from two tags in a package filled with books. We use three types of tags, Alien 964X, Impinj H47, and Impinj E41C. In Fig. 7 (a), (b), and (c), the experiment uses two tags that are with similar EPCs. While in Fig. 7 (d), (e), and (f), the experiment uses two tags with significantly different EPCs. We find that no matter the EPCs are close or not, Echoscope can always separate observations from two different tags. In order to avoid outliers and select the most stable features for each tag, we only choose the top-n candidate observations nearest to each cluster center in the two-dimensional space.

4.2 Environmental distortions reduction and signal pairing

After the signal collection and segmentation, we can get observations in two groups corresponding to the two tags respectively. From Equation (5), we know that environmental distortions can be reduced by computing the differences of pairs of values from these two groups. However, there are two challenges that are needed to be resolved.

1) Paring temporally adjacent observations. Though we have shown that the environmental noise will not contribute to a dominate factor by perform subtraction on the signals of two tags, we assumed that the pair of signals should be collected at about a same time. Since passive RFID systems usually use random-access algorithms, *e.g.*, the slotted ALOHA protocol, for anti-collision, observations are collected in different time slots. At one time point the monitor can only receive one the signal backscattered from one tag. However, external environments may be changed due to the movement of objects, such as a moving person or cart. selecting observations at very different time slots may fail to eliminate the noise from the external environment. Fortunately, since each time slot is very short (in the order of millisecond), we can expect that two backscattered signals in two close time slots experience the same environmental noise. Therefore, our first effort is to select two temporally adjacent observations for subtraction. Their time slots should be as close to each other as possible.

Using the method introduced in the previous subsection, Echoscope can tell the source of each observation. There are two approaches to select n pairs of observations: 1) The sys-

tem first decides the top n nearest observations to the cluster center of each tag. Then among the $2n$ observations of the two tags, the system selects m pairs, $m < n/2$, each of which includes two observations in two close-by slots. 2) Among all observations, the system selects m pairs, each of which includes two observations in two close-by slots. According to our experimental results, the first approach is more reliable and then used by Echoscope. Detailed experimental results are skipped due to the page limit.

The algorithm to compute the difference of the m pairs of observations is presented in Algorithm.1.

Algorithm 1 The algorithm to compute the m pairs of observations.

Input:
The top n nearest observations index of tag 1, I_1;
The top n nearest observations index of tag 2, I_2;
The slot interval threshold t;
The pointer for tag 1, p;
The pointer for tag 2, q;
Output:
The index set of observation pairs, S_o;

```
Sorting the index sequence I_1 and I_2 in the ascending order;
i = 1;
while i ≤ m do
    d = I_1(p) − I_2(q)
    if |d| ≤ t then
        S_o(i) = ⟨I_1(p), I_2(q)⟩
        i = i + 1;
    else if p − q < −t then
        p = p + 1;
    else
        q = q + 1;
    end if
    if i > minimum length of I_1 and I_2 then
        Break;
    end if
end while
return S_o;
```

2) Aligning the starting points of tag responses Another challenge to compute $S_1 - S_2$ for a pair of observations is to align their starting points of IDs. It is necessary because the IDs in different observations start at different time points. Note that each observation contains roughly 20,000 sampling points. Hence, using linear search and comparison is too complex to be efficient. Fortunately, the EPC C1G2 protocol specifies that each tag should delay its ID transmission for a tiny time duration after receiving an ACKThe value of this reply delay varies for different slots, but its length is usually about tens of sample points. This property helps to easily locate the desired start point from a sequence of sample points.

We use the change-point detection (CPD) mechanism to find the start point within each observation. Fig 8(a) illustrates an example of locating the start point. The essential idea of CPD is to detect a sharp change in a given curve. Let $EPC(m)$ be the m-th sampling point of the EPC. An intuitive way is to calculate forward difference $\Delta e = |EPC(m+1) - EPC(m)|$, and then check if Δe is higher than a threshold t, which is pre-determined by analyzing existing results.

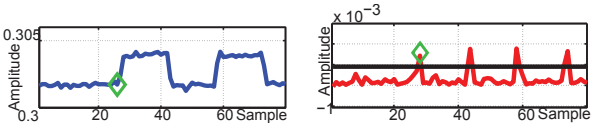

(a) Raw data of EPC (b) Curve of value Δe

Figure 8: Change point detection

In Fig 8(b), we plot the results of all values of Δe, where the black line is the value of threshold t. The start point, marked by the green square, is accurately located by checking whether $\Delta e > t$. Next, we arrange all the $(S_1 - S_2)$ results of observation pairs to an $m \times k$ feature matrix F. Here the m is the number of observation pairs and k is the amount of sample points of each EPC.

4.3 Feature extraction and matching

After signal pairing, we maintain a feature matrix F, where each row is a vector representing $(S_1 - S_2)$. To extract features that characterize the package internal status, we perform the discrete wavelet transform (DWT) on each row. A discrete signal S can be approximated by a combination of wavelet basis, while the coefficients of this combination can reflect the signal's characteristic. In our applications, the features of items are implied by the tags' responses. The output of DWT is two vectors: the approximation coefficients vector c_a and the detail coefficients vector c_d [1]. To choose an appropriate wavelet basis to analyze the raw data, we conduct two experiments. One is to compare the results of a same object at different locations, *e.g.* the check-in and test points. The other one is to compare the results using different objects. A good wavelet basis should increase the difference between different objects while shrinking the gap between the same objects. Fig. 9 shows the wavelet basis results from the same objects (alloys) at different locations. The raw data is divided into two vectors, *i.e.*, vector c_a and c_d. The blue curves and points represents results at the check-in site and the orange curves and points represents results at another testing site. db1, db7, db15, and db30 stand for different Daubechies wavelets. We find that the vector c_a of db15 has the best performance than other wavelet basis, because the results from different locations are very close. However, the c_d vectors of all the wavelet basis has no obvious similarity for different locations. To investigate the performance of db15 in distinguishing different objects, we depict the c_a vectors of db15 with different objects in the package. As shown in Fig.10, the gap between different materials are obvious and easy to distinguish. Hence, we employ $db15$ as the wavelet basis in the DWT processing. For each row in the feature matrix F, we use DWT to extract the approximate vector c_a. After this dispose, we have a new matrix D with size $m \times k'$, where m is the number of rows in the feature matrix F and k' is the length after performing DWT. Each row of D is a sequence of coefficient c_a.

By observing the DWT results of different materials in Fig.10, every material shows very different results in the vector c_a. We tried extracting the coefficient matrix D from the check-in and test results, use them as the train data and testing data respectively, and construct a classifier. However, the classification results are poor (accuracy $< 50\%$). The reason might be that the overall trend of the c_a changes plays a dominate role in classification. However, the details

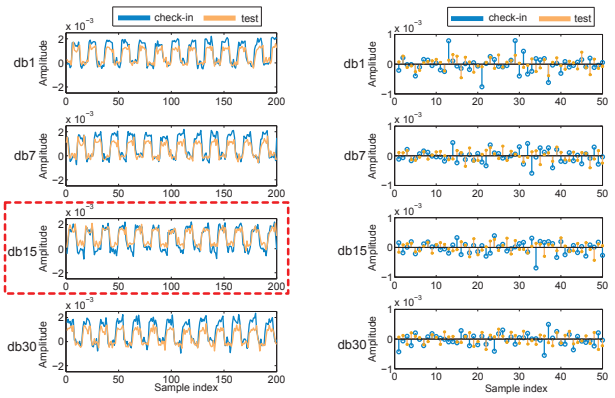

(a) c_a vectors (b) c_d vectors

Figure 9: c_a and c_d for different Daubechies wavelets.

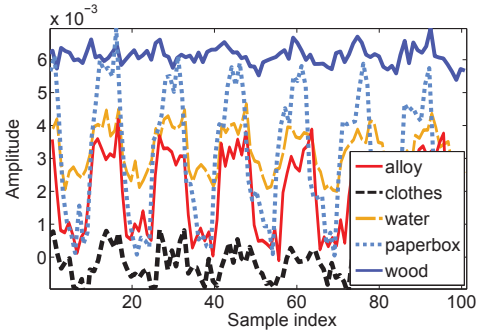

Figure 10: Vector c_a for different materials

of vector c_a are not reflected in the classifier. Under this consideration, we try to separate the trends V_t and small details V_d of coefficient matrix D. The method is shown as follows.

$$V_t(i) = \frac{\sum_{j=1}^{m} D(j,i)}{m}, 0 < i \leq k'$$
$$V_d(j,i) = D(j,i) - V_t(i), 0 < i \leq k', 0 < j \leq m \quad (8)$$

Then we have a trend vector $V_{t\ 1\times k'}$ and a detail matrix $V_{d\ m\times k'}$. As aforementioned, each row in matrix D represents a sequence of coefficient c_a, which extracts the characteristic from the feature matrix F. So, each row in the same matrix D should keep a stable characteristic and be similar with each other. The vector V_t reflects the mean level at each corresponding point of rows in matrix D. And matrix V_d keeps a record of the detailed variation at each point of every row. In this way, we can decompose the coefficient matrix D into two parts and compare them respectively. For comparing the V_t and V_d from samples collected in the check-in and test phases, we design an algorithm, *i.e.*, Algorithm.2, to make the final matching decision. The main idea of the algorithm is that if one of the similarities of $V_t and V_d$ is lower than the threshold, the package will be rejected. The result R is a Boolean number. If $R = 1$, we consider the internal status of the package has not been changed. If $R = 0$, we consider there may be changes of the internal status and further physical inspection will be conducted. This method takes the two parts of D into account and works very well in our experiments. We will show the results and threshold selection in next section.

Algorithm 2 Echoscope feature matching

Input:
The trend vector of samples in check-in, V_t^c;
The trend vector of samples in testing, V_t^t;
The detail matrix of samples in check-in, V_d^c;
The detail matrix of samples in testing, V_d^t;
The correlation threshold T;

Output:
The judgement result, R;

1: Calculating the cross-correlation coefficient x of vector V_t^c and V_t^t;
2: **if** $x \leq T$ **then**
3: $R = 0$;
4: **else**
5: Put V_d^c and V_d^t into a two-class Naive Bayesian classifier, and get predict result R.
6: **end if**
7: **return** R;

(a) Devices (b) Part of items

Figure 11: Experimental devices and filling materials

5. IMPLEMENTATION AND EXPERIMENTAL EVALUATION

We implement Echoscope using COTS devices and conduct experiments in practical environments to evaluate its performance.

5.1 Prototype system

An Echoscope prototype built with COTS devices is shown in Fig. 11(a). It consists of a commercial RFID reader model Impinj R220, a generic USRP monitor, and many tags. We use a USRP N210 plus an SBX daughterboard as the monitor. To show that Echoscope is ubiquitously applicable, we use three mainstream types of tags on the market, *i.e.*, Impinj E41C, Impinj H47 and Alien 964X. In the experiments, we attach two tags of a same type onto the bottom of each package, with the distance of 4cm in-between. Antennas (Laird S9028PCL) used by both the reader and monitor are circularly polarized with a gain of 8dBi. We use eight kinds of material to fill the internal space of the packages, including alloy, cloth, carton, glass, paper, plastic, water, and wood. Some of them are shown in Fig. 11(b).

5.2 Methodology

All experiments were conducted in the indoor environment where extensive RF noise exists, including WiFi, AM/FM, and Bluetooth signals. We use *different rooms in different buildings* to simulate the check-in and testing sites. We use three different sizes of cardboard packages as the containers. The three sizes are 17 cm×19 cm×29 cm (denoted as

"Small"), 23 cm×24 cm×40 cm ("Medium"), and 29 cm×37 cm×52 cm ("Large"). Note that all packages are *arbitrarily* selected and bought online. We did not determine their sizes in purpose.

For each set of experiments, we fill each package with one type of material and plastic foam for the remaining space. Items inside the package are arranged orderly and closed to each other without wrapped in other packing materials. In order to simulate the practice, we fill the package until all the items inside cannot move around more than *3cm* under violent shaking. The experiments are conducted in two phases, check-in and testing. In the check-in phase, Echoscope collects a *record* and computes the reference features for each package. And in the testing phase, we repeat the above steps and compare the features with that in check-in phase.

To evaluate our system, we utilize three suitable metrics, *i.e. accuracy*, *FAR* and *FRR*. In an experiment, if the objects in a package have not been changed and Echoscope reports `accept`$(R = 1)$, or the objects are changed and Echoscope reports `reject`$(R = 0)$, we consider this experiment is successful. The *accuracy* of Echoscope is defined as the ratio of successful ones among all experiments. Besides the accuracy, we also evaluate the false accept rate (*FAR*) and false reject rate (*FRR*) of Echoscope. The *FAR* is the ratio of unsuccessful ones among all experiments that report `accept`. *FRR* is the ratio of unsuccessful ones among all experiments that report `reject`. Obviously, the administrator of logistics systems may have more concerns on FAR than FRR, because false rejects can be avoided using extra testing methods which could be destructive. It is natural that if we suspect the items in a package are changed, we will eventually open the package to check. Hence under the same accuracy, we prefer lower FAR.

5.3 Impact of package size, tag distance, and threshold

We discuss the influences of the package size and distance between the two tags. We make use of 5 types of materials (alloy, water, book, clothes, and plastic) and put them into the three sizes of packages. We put the tag pair with a distance from 1cm to 6cm and illustrate the accuracy in Fig. 12(a) and Tab. 1. We find that the accuracy is always higher than 90% and FAR and FRR are mostly under 10%. According to the experiment results, it is recommended that for large packages the tag pair should have a distance of $5 \sim 6cm$. And for the small packages, the distance should be $2 \sim 4cm$.. In the next experiments, we utilize the package of the medium size with tags separated by 4cm.

By comparing the features, the threshold T in Algorithm 2 determines if Echoscope will accept or reject a package. We show the FAR, FRR, and EER (Equal Error Rate, happened when FAR equal to FRR) by varying T in Fig.12(b). Depending on different applications, Echoscope may select a proper T. For example, if we want to maximize the accuracy, we may choose $T = 0.47$ at the point of EER. If we want to have a smaller FRR, T should be smaller than 0.4.

5.4 Impact of environmental changes and moving objects

We conduct the experiments in both static and dynamic scenarios. In the static scenario we use a same Echoscope prototype (including the RFID reader and monitor) for both the check-in and testing phases. In the dynamic scenario we use different devices for check-in and testing. The static scenario simulates the inventory application in warehouses, and the dynamic scenario simulates the logistics applications across different transit stations. Note that to simulate a real logistic process, we always move the packages and shake them for several seconds before testing. In addition, we also introduce some *human impact*. We allow a volunteer walking around during the dynamic experiments. The region of his movement is from 20cm to 4m away from the package. The average moving speed is about 1.5m/s.

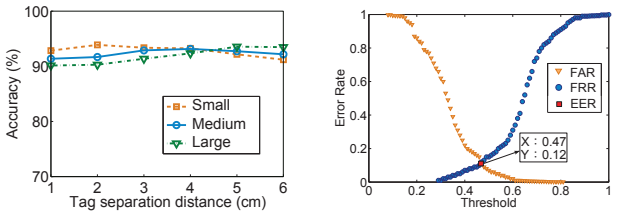

(a) Tag distance vs. accuracy (b) Threshold vs. error rates

Figure 12: Impact of package size, tag distance, and threshold

package	results	$1cm \sim 2cm$	$3cm \sim 4cm$	$5cm \sim 6cm$
Small	FAR	5.55%	6.67%	9.22%
	FRR	6.91%	6.70%	8.35%
Medium	FAR	6.11%	6.67%	10.00%
	FRR	7.82%	7.06%	6.93%
Large	FAR	16.67%	8.22%	4.44%
	FRR	8.07%	7.93%	7.00%

Table 1: Tag distance vs FAR and FRR

We show the accuracy of Echoscope in Fig. 13(a) and the FAR and FRR in Fig. **??** for three tag models and three scenarios: static, dynamic, and human impact. We fix the threshold for all experiments. We find that the accuracy is always higher than 90% in all cases. The FARs are smaller than 10% and FRRs are smaller than 5% using a fixed threshold. Among the three models of tags, we find that the Impinj H47 tags have the least FRRs (1.8% to 3.8% for three scenarios) and the FARs are as low as those of Alien tags (4.8% to 7.1%). In other words, only 4.8% to 7.9% packages whose internal objects are changed may not be detected by Echoscope. Echoscope is very robust to dynamic environments and noise introduced by surrounding moving objects.

5.5 Robust to various practical factors

We also conduct experiments to investigate the potential impacts of a number of practical factors.

5.5.1 *Sensitivity to displacement*

Note that in this work Echoscope deals with tightly filled and packed packages. Hence normal logistic operations (such as shaking and vibration) will only yield a small displacement, mostly less than 1cm. On the other side, abnormal internal changes can easily cause a relatively big displacement. Here we evaluate the sensitivity of Echoscope to the displacement of internal objects.

We use items with four types of material: paper, plastic, bottled water, and glass. For each experiment, we use one of

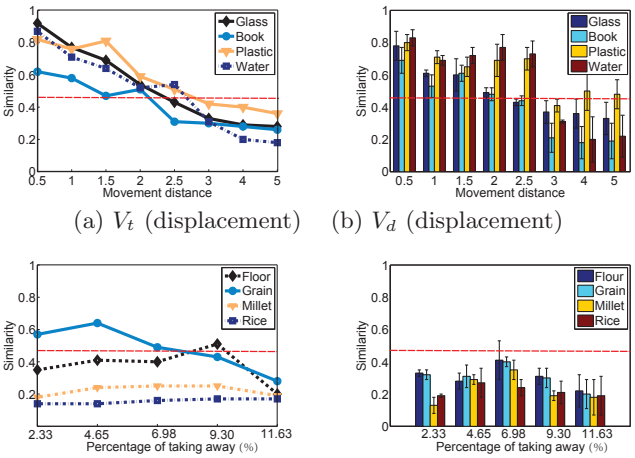

(a) V_t (displacement) (b) V_d (displacement)

(c) V_t (partial removal) (d) V_d (partial removal)

Figure 14: The average correlation coefficients after displacement or partial removal

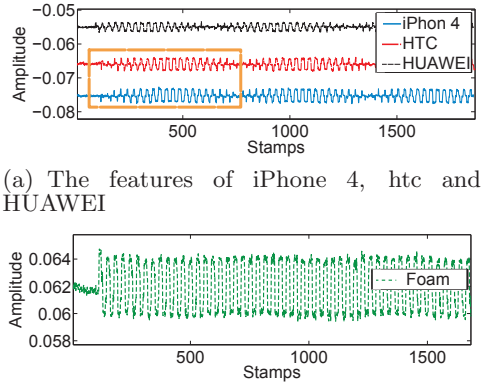

(a) The features of iPhone 4, htc and HUAWEI

(b) The features of the foam

Figure 15: Feature c_a of different types of items

five levels of displacement by changing the object positions from 1cm to 5cm. We investigate the cross-correlation coefficients of V_t and V_d respectively between the features of the check-in and testing phases, as the similarities. In this experiments, we set the threshold as $T = 0.47$ (the red lines). Note that if one of the similarities V_t and V_d is below the threshold, Echoscope will reject this package. We show in Fig. 14(a) and Fig. 14(b) the the cross-correlation coefficients of V_t and V_d for all materials as well as the threshold (in red lines). When the displacement is within 1cm, Echoscope will accept all packages. When the displacement is larger than 3cm, Echoscope will reject all packages. According to life experience, a displacement larger than 3cm would be obvious in packages. Therefore in practice normal logistic operations will not cause the package to be rejected. In addition, large displacement will be aware to Echoscope. Note that abnormal object changes will not just cause displacement and we will show more results of them.

5.5.2 *Sensitivity to partial removal or substitution*

Attackers may take a part of items in a package, instead of taking all items away. We exam the ability of Echoscope to detect such partial removal or substitution.

We fill a medium size package with one of the four kinds of goods, *i.e.*, flour, grain, millet, and rice. We record the features in the check-in phase and then take away a part of them before performing testing. The similarities (in cross-correlation coefficients) of check-in and testing features are shown in Fig. 14(c) and Fig. 14(d). The results show that, even only 2.33% taking-off will be recognized by Echoscope and the package will be rejected.

We observe similar results for partial substitution. Thus, Echoscope is very sensitive to partial removal and substitution.

5.5.3 *Sensitivity to different items with same material*

We now consider another status change of a package. An attacker may substitute the original items with items made in same material, for example, replacing the original wines by much cheaper ones. We conduct our experiments using three types of items (as shown in Fig. 11(b)), including smart phones, wines, and cigarettes. For each type of items, we replace the original items with another brand (not exactly in the same weight and shape as the original one) and test whether Echoscope can correctly report these changes. The results are shown in Table 2. The most important metric is the FAR that quantifies the false-acceptances by Echoscope after substitution. For the wines and cigarettes, the FAR is very low (4.51% and 3.54% respectively). The FAR is higher for smart phones, but Echoscope can still detect most package changes.

We conduct an experiment with three cellphones, *i.e.*, iPhone 4, HTC S510e and HUAWEI G7, and a foam. The foam and HTC have the same shape with iPhone 4. And the HUAWEI is the same weight with iPhone 4. We depict the C_a vector of these four items after performing DWT in Fig. 15. We find that the C_a vectors are quite different among HUAWEI, foam plastics and iPhone 4. However, it is a little difficult to distinguish iPhone 4 and HTC. The C_a vectors are similar for these two items. Thus Echoscope can find out the things with different shapes and materials easily. As comparison, X-ray cannot distinguish iPhone 4 from the foam, the weighting method cannot tell the difference between HUAWEI and iPhone, and the seal tag method cannot distinguish all of these substitutes.

6. DISCUSSION

Signal penetrability: Echoscope can work in the presence of signal blockage. If the signal is blocked, it is still diffracted and refracted around the internal items. Such diffraction and refraction can also enable the feature extraction and matching to our approach. For items with strong blocking effect on the RF signal, we suggest to increase the transmission power or employ the tags with better backscattering capacity, e.g., anti-metal tags.

Container materials: We choose paper-based boxes in the experiments because most containers in real-world logistic and storage are made by paper. On the other hand, we did evaluate the performance of Echoscope in detecting contents with common materials, such as wood, glass, plastics, and alloy. We found that the RF signals is able to penetrate these materials and distinguish them. Since the container can be considered as a part of the item, the results imply that the material of containers has negligible influence to our system.

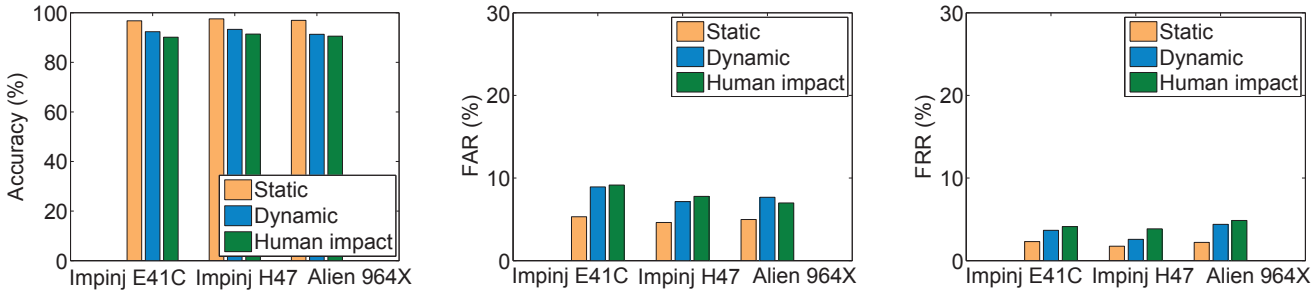

(a) Accuracy for different environments (b) FAR (c) FRR

Figure 13: Impact of dynamic environments and moving objects

material	Accuracy	FRR	FAR
Phone	94.11%	2.87%	8.56%
Cigarette	98.76%	2.06%	3.54%
Wine	97.89%	1.77%	4.51%

Table 2: The experiment result of similar objects

7. RELATED WORK

A number of technologies have potentials to be the alternatives of Echoscope, including radar, thermography and WiFi. Radar is an object-detection system that uses radio waves to determine the range, angle, or velocity of objects [18] [11] [2]. However, it requires much more complex and bulky devices and is subject to licensing and regulations (due to larger frequency bandwidth). Thermography uses infrared spectroscopy [19] to achieve high resolution on the produced images. However it is also imagery based. Besides the privacy concern, it has the limitations in the high expense of the larger pixel array and low interpretation accuracy upon erratic temperatures. WiFi based object recognition is also a potential solution but not practical for the application of this work. It is because the diversity of WiFi devices, such as APs and wireless NICs, introduces significant errors to the features extracted from the signals. Trustworthy and low-cost RFID have been studied for various applications and platforms [3]. Among these works, Danev *et al.* [5] focus on identifying HF tags using physical-layer information. Methods proposed in [23] [14] [25] are physical-layer identification for UHF tags. These approaches all focus on identifying tags, because it is generally assumed that tracking tags is equal to tracking the objects they attach to.

Recently, a growing number of studies start to investigate the identification and tracking of real objects or human beings, rather than their tags. In the areas of RF-based sensing, a lot of research projects have been conducted on detection of human motion or static metallic objects, such as those in [16] [21] [26]. Specifically, [16] [21] provide methods that utilize 500 MHz to 3 GHz wideband transmissions to detect human motion and image metallic objects. However, these works rely on expensive and specialized devices, which may limit their widespread uses. A number of systems are proposed to leverage wireless signals to detect and sense human actions such as running, moving and human gesture [22] [15] [24] [10] [4] [9] [17]. However, none of them is designed for nondestructive testing.

8. FUTURE WORK

Echoscope is mainly used to verify whether the internal status of a package is changed or not. The information about this package, e.g., what contents are in this package, is known in advance. We speculate that Echoscope has an ability to perform such identification. Indeed, our experiments and evaluation part show Echoscope's ability in distinguishing different materials. However, the accuracy of such identification needs further investigation and evaluation.

Echoscope has a limitation that packages should be tightly filled and packed. That is a constraint and disqualifies a majority of applications. We will investigate to release this constraint in our future work.

We admit that our technique requires exact placements of the two antennas. In practice, this problem can be solved by utilizing pre-printed package with certain markers for antenna alignment. We will increase the tolerance of antennasáŕ positions in our future work.

9. CONCLUSION

We design and implement the first nondestructive package testing and verification system using COTS RFID devices, called Echoscope. We successfully demonstrate that analysis on backscatter signals may reveal internal status of packages, by both theoretical modelling and experimental results. We design novel methods to segment backscatter signals, recognize the source of signals, find pairs of signals to eliminate noise, and perform feature matching. The evaluation results based on prototyping in practical environments show that Echoscope has very high accuracy to detect abnormal intern changes and low false accept rate. Echoscope works well for a large variety of materials, in both static and dynamic environments with surrounding moving objects.

10. ACKNOWLEDGMENT

This work was supported in part by National Basic Research Program of China (973 Program) under Grant No. 2015CB351705, NSFC Grant No.61190112, 61325013, 61572396, 61402359, China 863 Grant 2013AA014601, and National Science and Technology Major Project of the Ministry of Science and Technology of China JZ-20150910. Chen Qian is supported by UC Santa Cruz Startup Grant and National Science Foundation grant CNS-1464335. We thank the valuable comments from anonymous reviewers.

11. REFERENCES

[1] P. Addison. The illustrated wavelet transform handbook. *Science Engineering Medicine , Finance Institute of Physics Publishing*, 2002.

[2] P. Bahl and V. N. Padmanabhan. RADAR: An in-building RF-based user location and tracking system. In *Proceedings of IEEE INFOCOM*, 2000.

[3] V. Brik, S. Banerjee, M. Gruteser, and S. Oh. Wireless device identification with radiometric signatures. In *Proceedings of ACM MOBICOM*, 2008.

[4] K. Chetty, G. E. Smith, and K. Woodbridge. Through-the-wall sensing of personnel using passive bistatic WiFi radar at standoff distances. *IEEE Transactions on Geoscience and Remote Sensing(GRS)*, 50(4):1218–1226, 2012.

[5] B. Danev, S. Capkun, R. Jayaram Masti, and T. S. Benjamin. Towards practical identification of HF RFID devices. *ACM transactions on Information and System Security (TISSEC)*, 15(2):7, 2012.

[6] E. Gen. EPC radio-frequency identity protocols class-1 generation-2 UHF RFID protocol for communications at 860 MHz–960 MHz, 2008.

[7] G. Grimmett and D. Stirzaker. Probability and random processes. *Oxford University Press*, 1982.

[8] W. H. Hayt and J. A. Buck. *Engineering electromagnetics*. McGraw-Hill New York, 2001.

[9] D. Huang, R. Nandakumar, and S. Gollakota. Feasibility and limits of Wi-Fi imaging. In *Proceedings of ACM SenSys*, 2014.

[10] B. Kellogg, V. Talla, and S. Gollakota. Bringing gesture recognition to all devices. In *Proceedings of USENIX NSDI*, 2014.

[11] F. E. Nathanson, J. P. Reilly, and M. N. Cohen. Radar design principles-signal processing and the environment. *NASA STI/Recon Technical Report A*, 1991.

[12] L. M. Ni, Y. Liu, Y. C. Lau, and A. P. Patil. LANDMARC: indoor location sensing using active RFID. *Wireless Networks*, 10(6):701–710, 2004.

[13] J. Ou, M. Li, and Y. Zheng. Come and be served: Parallel decoding for COTS RFID tags. In *Proceedings of ACM MOBICOM*, 2015.

[14] S. C. G. Periaswamy, D. R. Thompson, and J. Di. Fingerprinting RFID tags. *IEEE transactions on Dependable and Secure Computing(TDSC)*, 8(6):938–943, 2011.

[15] Q. Pu, S. Gupta, S. Gollakota, and S. Patel. Whole-home gesture recognition using wireless signals. In *Proceedings of ACM MOBICOM*, 2013.

[16] T. S. Ralston, G. L. Charvat, and J. E. Peabody. Real-time through-wall imaging using an ultrawideband Multiple-Input Multiple-Output (MIMO) phased array radar system. In *Proceedings of IEEE ARRAY*, 2010.

[17] S. Sigg, S. Shi, and Y. Ji. RF-based device-free recognition of simultaneously conducted activities. In *Proceedings of ACM UbiComp*, 2013.

[18] M. I. Skolnik. Introduction to radar. *Radar Handbook*, 1962.

[19] B. Stuart. *Infrared spectroscopy*. Wiley Online Library, 2005.

[20] J. Wang and D. Katabi. Dude, where's my card?: RFID positioning that works with multipath and non-line of sight. In *Proceedings of ACM SIGCOMM*, 2013.

[21] Y. Wang, M. J. Kuhn, and A. E. Fathy. Advanced system level simulation of UWB three-dimensional through-wall imaging radar for performance limitation prediction. In *Proceedings of IEEE MTT*, 2010.

[22] L. Yang, Y. Chen, X. Li, C. Xiao, M. Li, and Y. Liu. Tagoram: Real-time tracking of mobile RFID tags to high precision using COTS devices. In *Proceedings of ACM MOBICOM*, 2014.

[23] D. Zanetti, B. Danev, et al. Physical-layer identification of UHF RFID tags. In *Proceedings of ACM MOBICOM*, 2010.

[24] Y. Zheng and M. Li. Open RFID lab. Available: http://pdcc.ntu.edu.sg/wands/ORL, 2013.

[25] Y. Zheng and M. Li. P-mti: Physical-layer missing tag identification via compressive sensing. In *Proceedings of IEEE INFOCOM*, 2013.

[26] F. Zhu, S. Gao, A. T. S. Ho, T. W. Brown, J. Li, and J.-D. Xu. Low-profile directional ultra-wideband antenna for see-through-wall imaging applications. *Progress In Electromagnetics Research*, 121:121–139, 2011.